

# Characterizing the Mechanics of Fracturing from Earthquake Source Parameter and Multiplet Analyses: Application to the Soultz-sous-Forêts Hot Dry Rock site

Sophie Michelet, Nafi Toksöz  
Earth Resources Laboratory  
Dept. of Earth, Atmospheric and Planetary Sciences  
Massachusetts Institute of Technology  
Cambridge, MA 02139

## Abstract

In 2000 and 2003, two massive hydraulic fracturing experiments were carried out at the European Geothermal Hot Dry Rock site at Soultz-sous-Forêts, France. The objective was to create a dense network of enhanced permeability fractures, which would form the heat exchanger. The injection of water in the fractured rock generated a high level of microseismic activity: around 30,000 and 90,000 micro-earthquakes were triggered during the injection of 2000 and 2003 respectively. From this around 14,000 and 9,000 events were then located to characterize the extent of the stimulated zones and hence of the fracture network. Then, the source parameters of each event, like seismic moments and stress drops, were computed automatically to characterize the mechanics of the fracturing. We found for example that the total seismic moment released is proportional to the injected fluid volume. This suggests that the injection flow rate could be a means to control the earthquake strength released during the stimulation and perhaps also control the effectiveness of the stimulation. Finally, we performed a multiplet analysis of a subset of these data to identify microearthquakes having similar waveforms. Multiplets are considered to be microearthquakes that occur on the same fracture plane and therefore may represent either seismically activated structures and/or permeable fractures induced by hydraulic fracturing. We identified 350 multiplets among 1000 analyzed events. We relocated them precisely by cross-spectrum analysis and found that they belong to sub-horizontal structures, likely permeable fractures stimulated by the injection.

## 1. Introduction

The Hot Dry Rock concept consists of extracting heat energy from the ground by circulating water through pre-existing fractures between two boreholes at great depth (several kilometers). In order to create a dense and permeable fracture network, a hydraulic fracturing experiment is performed to stimulate the hot, low permeability rock. This operation induces a large number of microseismic events, typically more than one hundred events per hour. The location of the microearthquakes allows determining the extent of the stimulated zone and hence of the fracture network (Block et al., 1994, Phillips et al., 1997, Li et al., 1998). Besides, the source mechanism of the microseismic events (e.g. fault plane solutions and source parameters) permits us to characterize the geometry and the mechanics of the stimulated fractures (Fehler and Phillips, 1991).

In the present study, we computed automatically source parameters of more than 14,000 microearthquakes generated during the hydro-fracturing of the Soultz-sous-Forêts geothermal reservoir. We will show how such parameters can be used to characterize the mechanical response of the reservoir to the hydraulic fracturing. On a second study, we compared the waveforms of the microearthquakes to identify similar events. Such events are called multiplets and are considered to be the expression of stress release on the same fracture. This analysis was only performed on a subset of the data (~ 1000 events) because it is very computer-time-consuming. Then, we determined the relative locations of the multiplets by cross-spectrum analysis to evaluate the distribution and orientation of fractures (Poupinet et al., 1984; Moriya et al., 1994; Tezuka and Nitsuma, 1997; Gaucher et al., 1998).

## 2. Seismicity associated with hydraulic fracturing

The European Hot Dry Rock research site is situated about 50 km north of Strasbourg, in the Northern flank of the Rhine Graben, which is part of the Western European rift system (Figure 1). This graben consists of a granite basement that is covered by sedimentary layers about 1400 m thick. Baria et al (2004) gives a brief summary of the various stages of the development of this technology at Soultz since 1987. Main aspect of the project involves

the hydro-fracturing (i.e. stimulation) of different wells at different depths, the characterization of the well performance and the monitoring of the associated microseismicity. In this study we deal with the induced seismicity.

## 2.1 Stimulation of the year 2000

Between 30<sup>th</sup> June and 6<sup>th</sup> July 2000, a total volume of 23,400 m<sup>3</sup> of water was injected between 4430m and 5085m measured depth (figure 2a) to stimulate the GPK2 well. With the objective of enhancing the permeability of the deepest, and the hottest, section of the granite, the stimulation was initiated by injecting saturated brine at a flow rate corresponding to a pressure above that required for the onset of stimulation. Having started the stimulation process using this heavy injection fluid, the stimulation continued with the injection of fresh water. After this initial period during which a flow rate of 31 l/s was maintained, the rate was increased to 41 l/s and then 51 l/s.

A comprehensive seismic monitoring system was set up and operated during the injection and after the shut-in of the wells (figures 1 & 3): hydrophones were deployed in wells GPK-1 and EPS-1 (3499m and 2017m depth, respectively) and 4-axis accelerometer tools in the observation wells 4601, 4550 and OPS-4 (1539m, 1482m and 1485m depth, respectively). All these seismic sensors were installed below the granite-sediments interface in order to remove surface effects owing to the attenuation and scattering of the sedimentary layers.

During the monitoring period, 31,511 triggers were recorded at a sampling rate of 2000 Hz on the down-hole network from which 13,954 events were located and processed (figure 2b). The seismic activity was high throughout the entire experiment (more than one hundred events per hour). After shut-in, it decayed rapidly but a significant event rate persisted (around ten events per hour). The seismic cloud trended northwest of the well GPK2 and extended from the casing shoe (i.e. 4430m) to 5500m depths. This orientation is in accordance with the orientation of the acting major horizontal stress (N30W) obtained by Hettkamp et al. (1998). The moment magnitudes of these microearthquakes ranged between -2 and 2.6. Actually, the largest one occurred one week after the end of the injection.

## 2.2 Stimulation of the year 2003

Between 27<sup>th</sup> May 2003 and 6<sup>th</sup> June 2003, a total of 34.000 m<sup>3</sup> was injected into GPK-3 at flow rates up to 95 l/s. During the stimulation test, 90,648 triggers were recorded at a sampling rate of 2000Hz on the down-hole network from which 21,634 events were located (See figure 7). Here again, the seismic activity was high throughout the entire experiment with an average of 300 events per hour and a maximum rate of 580 events per hour just after the flow rate of 93 l/s. The seismic rate during the 2000 stimulation was not that high because the threshold trigger was higher than in 2003. After the shut-in of the well GPK-3, the number of events per hour decreased but the seismic activity was still high (more than 100 events per hour) and three microseismic events of local magnitude ranging between 2.9 and 2.7 happened. The seismic cloud has approximate dimensions of 1.5 by 2.5 by 1.5 km, striking N30W, which is again in accordance with orientation of the acting major horizontal stress (Hettkamp et al, 1998).

## 3. Source parameter calculation

### 3.1 Theory

The seismicity from the 2000 stimulation is analyzed here. Three accelerometers, deployed in wells 4550, 4601 and OPS-4, were used to compute the particle acceleration associated to the seismic waves. Because of a periodic noise on the traces of the accelerometer in well 4550, the traces were unusable. Therefore, we only processed the records of the sensors in wells 4601 and OPS-4.

We worked with the P arrivals on the vertical sensors because we can reasonably assume that the P-wave has a vertical angle of incidence. Indeed, the mean incidence angle of the events at both stations is less than ten degrees. The vertical trace from each station was then windowed with a window of 300ms containing the P pulse and beginning at the picked P-wave arrival time and then Fourier transformed to give the corresponding acceleration spectrum (figure 4).

We assumed that the Brune's model (an  $\omega$ -squared fall-off of the high frequency displacement spectrum above a single corner frequency) is an adequate description of the earthquake source (Brune, 1970). We therefore

considered that the following model spectrum  $M(f)$  is a smooth approximation for the observed acceleration spectrum  $A(f)$

$$M(f_i) = A_0 * \frac{(2\pi f_i)^2}{\left(1 + \left(\frac{f_i}{f_0}\right)^\gamma\right)} \quad (1)$$

where  $\gamma$  gives the fall-off of the spectrum at high frequencies,  $f_i$  is the frequency of radiated energy and the subscript  $i$  signifies that the model is evaluated at discrete frequency points.  $A_0$  is the low-frequency limit of the acceleration spectrum, also called plateau. Following Brune (1970), we assume  $\gamma = 2$ .

We took into account the effect of attenuation on the spectral decay at high frequencies because it can dramatically affect the determination of the corner frequency (Anderson and Humphrey, 1991). We therefore assumed that the observed acceleration spectrum is described by

$$A(f_i) = M(f_i) * e^{-\pi\kappa f_i} \quad (2)$$

where  $\kappa$  is the high frequency spectral decay parameter (s). Anderson (1986) suggested that the most appropriate value for  $\kappa$  is defined by

$$\kappa(f_i) = \frac{R}{Q(f_i) * \alpha} \quad (3)$$

where  $R$  is the distance source-sensor (m),  $\alpha$  is the P-wave velocity ( $\text{m.s}^{-1}$ ) and  $Q$  is the quality factor. Here, we followed Anderson (1986) and assumed that the quality factor  $Q$  is independent of frequency and hence that  $\kappa$  is constant. Therefore, we fit the acceleration spectrum of the P-wave using (2) where the unknowns are the low frequency limit  $A_0$  (N.m), the corner frequency  $f_0$  (Hz) and the spectral decay parameter  $\kappa$  (s). It is not possible to set up a linear algorithm to obtain all three parameters simultaneously. Therefore, we first determined a constant value of  $\kappa$  for all the data by fitting the model on randomly selected events. We then determined  $A_0$  at low frequencies where the data are not affected too much by the attenuation. Finally, we determined  $f_0$  by selecting the value that minimized the misfit between the model and the observed spectrum using a Root Mean Square function. We made that fit automatically for all the data.

As can be seen in figure 4, the spectra were fitted with relation (2) between 30 and 400 Hz because, for higher frequencies, the noise was greater than the signal (Jones and Evans, 2001). We estimated a  $\kappa$  of  $4.5 \text{ ms} \pm 0.5 \text{ ms}$ , which corresponds to a  $Q$  of about 140. We would like to point out that it is very important to have a good estimation of the attenuation factor otherwise the corner frequency and the stress drop will be incorrectly estimated. Indeed, the corner frequency occurs at a frequency where attenuation has a strong effect on the spectrum. Anderson (1986) showed that in the case of small earthquakes, the corner frequency picked from the spectrum would underestimate the true corner frequency. Hence, an underestimate of the corner frequency would lead to an underestimate of the stress drop.

From the three unknowns of the source model, we computed the seismic moment, the source radius, the stress drop and the average slip of the microseismic event (Brune, 1970). In testing our algorithm on synthetic spectra with Gaussian noise, we arrived at the conclusion that it was possible to obtain the appropriate corner frequency with a misfit of  $\pm 10 \text{ Hz}$  and the plateau at  $\pm 0.05 \cdot 10^{-11} \text{ m.s}$ . The seismic moment has therefore an inaccuracy of  $\pm 3.1310^7 \text{ N.m}$ , the source radius of  $\pm 1.06 \text{ m}$ , the stress drop  $\pm 0.2 \text{ MPa}$  and the average slip of  $\pm 9.4 \cdot 10^{-5} \text{ m}$ . These errors are inherent in the inversion scheme and are not representative of the random errors on the actual data.

## 3.2 Results

### a) Seismic moment

We prefer to present seismic moments rather than moment magnitudes because no properly calibrated moment magnitude relationship is available in Soultz-sous-Forêts. On figure 5, we show the spatial distribution of the seismic moment for events that occurred before and after shut-in (blue and red, respectively). The events with the largest seismic moments are recorded during the stimulation, close to the injection well. Surprisingly, after the end of the injection, large events still occurred far away from the well. This is especially the case in a small area in the North of the cloud at a depth of 4400m. We would like to point out that the largest event of M12.6 occurred at this location one week after the shutdown of the injection pumps. This suggests that the seismic moment distribution

highlights areas where the seismic activity is potentially high. This feature has been confirmed by the following stimulation experiments performed in 2003 when a M12.9 earthquake occurred (Michelet et al., 2003).

*b) Total seismic Moment versus injection rate*

Figure 6 represents the total seismic moment released (N.m) versus the injected fluid volume (m<sup>3</sup>). We observe a clear linear relation between these two parameters. This suggests that the injection flow rate could be a means to control the earthquake strength released during the stimulation and perhaps also control the effectiveness of the stimulation. Indeed, for instance, if during a stimulation experiment, too much mechanical energy is being released, decreasing the flow rate should reduce the level of seismic activity. In Rangely (Colorado), Nicholson and Wesson (1992) showed that manipulating of the fluid injection pressure allows controlling the behavior of a large number of induced microearthquakes. Nevertheless, at the Rocky Mountain Arsenal (Healy et al, 1968), after the end of injection, earthquakes persisted for months and one M5 event was observed one year later. Therefore, seismicity can eventually be stopped in a number of cases either by ceasing the injection or by lowering pumping pressures but, as the Rocky Mountain Arsenal experiment showed it, this rule is not universal.

Following McGarr (1976), the most straightforward measure of ground deformation in the case of microseismic events induced by water injection at depth, is the total volume of injected water. He found a *linear* relation between the volume changes  $\Delta V$  and the total seismic moment  $\Sigma M_0$ :

$$\sum M_0 = K \cdot \mu \cdot |\Delta V| \quad (4)$$

where K is a factor ranging between  $\frac{1}{3}$  and  $\frac{4}{3}$  and  $\mu$  is the modulus of rigidity (N/m<sup>2</sup>).

The value  $K \cdot \mu \cdot |\Delta V|$  is termed the *volumetric moment*. It is a measure of the seismic failure that occurs in response to the shear stresses induced by a volume change  $\Delta V$ . In our case, the coefficient  $\Sigma M_0 / \Delta V$  is between  $4 \cdot 10^9$  Pa (sensor in well 4601) and  $4.8 \cdot 10^9$  Pa (sensor in well OPS4) where  $\Delta V$  is simply the volume of injected fluid. So, substituting values in relation (4), we found K equal to 0.37. To interpret this value, we make the approximation that our K is close to  $\frac{1}{3}$ . According to McGarr, in this case, volume is added to the region resulting in expansion in the stress components  $\sigma_2$  (intermediate stress) and  $\sigma_3$  (minimum stress). This is indeed what is observed in Soultz-sous-Forêts because  $\sigma_2$  is NW-SE and  $\sigma_3$  NE-SW and the cloud has an elliptic shape elongated in NW-SE direction.

*c) Stress drop and source radius*

We observed that high stress drops after the shutdown of the wells were located at the edges of the cloud. We can interpret this behavior as a stress front propagation from the well out into the reservoir. Thus, events with the largest stress drops occurred near the edges of the seismically active zone where newly activated faults may be expected rather than in the interior of the seismic zone, which has already been fractured (Fehler and Phillips, 1991).

Source radii were also computed; they represent the radius of the fault plane that is slipping during the earthquake. Following Madariaga (1976), it is assumed that the fault plane is circular. Most of the radii range between 4 and 10 meters.

## 4. Multiplet analysis

### 4.1 Detection of multiplets

The seismicity from a subset of the 2003 stimulation is analyzed here (in dark green on figure 7). Here we regard events that have nearly identical waveforms as a multiplet. We define the multiplet as being a group of seismic events whose P and S onsets and several periods of waves exhibit a high cross correlation (Moriya et al, 2002).

We used the normalized cross spectrum to measure the similarity between two time series. We calculated coherency function on a window starting at the P arrival time for a length of 128 ms to exclude the coda waves. The calculation of this coherency was carried out using the vertical component of the geophone in well EPS1. We decided to use this sensor because the signals at #EPS1 have the highest signal/noise ratio and because it is located further away from the heterogeneous sediment layers than the other seismic sensors. Then, we averaged the coherency between 60 and 190 Hz because most of the seismic energy is found around 100 Hz. A group of seismic events with an averaged coherency above 0.8 was regarded as initial candidates for multiplets. Then, through visual observation, we selected only the events that have very similar P- and S-wave onsets of waveforms. Figure 8 shows the waveforms of one of these multiplets.

We computed the coherencies between 1112 events that occurred in the area where the highest seismic activity was observed (figure 7). As a result, a total of 350 events were classified as doublets and multiplets. We decided to compute the relative locations of clusters with 4 events and more. So, we ended up with 12 clusters composed of 70 events of good quality. Several clusters were disregarded due to noisy waveforms, especially for the waveforms recorded at the sensor in well ops4. The interval between two events of a cluster was found to be in general less than few hours, and for most of them, few minutes. This observation reinforces the hypothesis that these events belong to the same stimulated fracture.

## 4.2 Relative Source location

As our objective was to locate events with the accuracy of a few meters, we decided to use P and S-waves (Moriya et al., 1994). This leads to a more laborious work but fortunately much more precision.

A multiplet is relocated from a set of time delays computed for each doublet in it. In our case, we worked in the Fourier domain involving that the time delay is proportional to the slope of the cross-spectrum phase. For one doublet, the computation of the time delay is done by fitting a weighted line to the phase of the cross-spectrum. The stability of this time delay is analyzed by moving a window successively within the P-wave train.

Figure 9 shows the measurement of the time delay for the P train between two seismograms. The phase of the cross-spectrum is computed from a 128 ms window starting at the P arrival (figure 9b). Then, the delay is obtained by fitting a straight line at the origin through the values of the phase using a least squares method. Each point is weighted by a factor proportional to the coherency between the two signals (figure 9a). The use of a weight optimizes the time delay resolution. It accentuates signals at frequencies for which the signal/noise ratio is high. The closer to 1 the coherency is, the larger the weight is. We can observe that the coherency is between 0.8 and 1.0 in the frequency band 40-200 Hz, therefore the time delay is determined in this interval and found to be -0.5ms for this example. In a second time, we aligned the two traces using the delay time calculated previously (figure 10).

Having aligned the two traces, the same procedure is used to compute the delay at the S wave arrival. Once again, the time delay is obtained by fitting the phase. The method used to relocate one event relatively to a reference event is based on a grid search algorithm. The objective is to find the increments  $\Delta x$ ,  $\Delta y$  and  $\Delta z$  to go from the reference event to the slave event. Assuming a homogeneous medium, the distance  $\Delta L$  between two events A and B is

$$\Delta L = \frac{(t_S^A - t_P^A) - (t_S^B - t_P^B)}{\frac{1}{V_S} - \frac{1}{V_P}} \quad (5)$$

where  $t_s^A, t_p^A, t_s^B, t_p^B$  are the arrival times for the S and the P waves of the events A and B respectively;  $V_p, V_s$  are the P and S wave velocities..

For a given station, these arrival times can be expressed as:

$$t_S^A = t_0^A + \sqrt{(x_A - x_{station})^2 + (y_A - y_{station})^2 + (z_A - z_{station})^2} / V_S \quad (6)$$

$$t_P^A = t_0^A + \sqrt{(x_A - x_{station})^2 + (y_A - y_{station})^2 + (z_A - z_{station})^2} / V_P \quad (7)$$

where  $t_0^A, x_A, y_A$  and  $z_A$  are respectively the origin time, the hypocenter coordinates of the event A.

Therefore, the P and S arrival times for the slave event B are:

$$t_S^B = t_0^B + \sqrt{(x_A + \Delta x - x_{station})^2 + (y_A + \Delta y - y_{station})^2 + (z_A + \Delta z - z_{station})^2} / V_S \quad (8)$$

$$t_P^B = t_0^B + \sqrt{(x_A + \Delta x - x_{station})^2 + (y_A + \Delta y - y_{station})^2 + (z_A + \Delta z - z_{station})^2} / V_P \quad (9)$$

where  $(\Delta x, \Delta y, \Delta z)$  are the distance between the events in the x-y- and z- directions and  $t_0^B$  the origin time for the event B.

Hence, the theoretical delay between the two microearthquakes A and B is:

$$d_{diff} = t_P^A - t_P^B - (t_S^A - t_S^B) \quad (10)$$

Consequently, we have to minimize the difference between the theoretical and the observed delay. To do so, we used a Root Mean Square error function, defined as:

$$\Delta = \frac{1}{\sqrt{n}} \sum \sqrt{(d - d_{diff})^2} \quad (11)$$

where  $d$  is the observed delay time for the doublet at each station and  $n$  is the number of observations. We minimized this error function using a grid search algorithm. For our example, the  $S$  delay was found to be 0.3ms, corresponding to a relative distance of about 2.4m.

### 4.3. Evaluation of detailed structure

This procedure was done for the 12 clusters and the figures 11 and 12 show the relocated microearthquakes on vertical and map views. In our case, the location of the reference event was chosen to be the centroid of the absolute locations of the other events of the cluster. The size of the clusters is small, events are really close to each other: their extent is less than 50m and is in general about 10s of meters. They trend North with varying dips.

The largest cluster is composed of 19 microearthquakes and we decided to take a closer look at their amplitudes. Figure 13 represents these 19 events as spheres with radii proportional to their amplitudes. Surprisingly, the larger microearthquakes occur at the edge of the structure. These events form a sub-horizontal planar shape (with a dip of 7 degrees). We generally assume that fractures will be vertical and have dips of about 60-90 degrees. What we find here changes the conception of large vertical features in a fractured reservoir.

Multiplets are considered to be microearthquakes that occur on the same fracture plane, yet there is a possibility that the structural planes identified by the multiplet sources represent either seismically activated structures and/or fractures induced by hydraulic fracturing (Moriya et al, 2002). Therefore, in the near future, we will apply the principal component analysis on our data to evaluate the shape and the source distribution of each multiplet cluster.

## 5. Conclusion

The hydro-fracturing of the Soultz-sous-Forêts fractured reservoir generated a high level of microseismic activity. From this around 14,000 and 9,000 events were then located to characterize the extent of the stimulated zones and hence of the fracture network. A large number of microearthquakes were located and processed automatically to characterize the source parameters. These parameters are essential to understanding properties of the reservoir. For example, the knowledge of the seismic moment could be a possible way of controlling the seismicity and the extension of the stimulated zone. Besides, the analysis of the events with similar waveforms enables to monitor the dynamic behavior of stimulated fractures. Indeed, such events are considered to be the expression of stress release on the same fracture. This technique will lead us to characterize the evolution of the stress field during the stimulation and hence to monitor the pore pressure within the fractures.

## 6. Acknowledgements

This work was partially supported by the ERL Founding Member Consortium. The authors would like to thank R. Baria, S. Oates, and B. Dyer. A special thank goes to M. Darnet for his constructive comments.

## References

- Anderson, J.G. and Humphrey, J.R., 1991, A Least Squares Method for Objective Determination of Earthquake Source Parameters, *Seismological Research Letters*, 62, No 3-4, 201-209
- Anderson, J.G., 1986, Implications of Attenuation for Studies of the Earthquake source, in S. Das, J. Boatwright, and C.H. Scholz, eds, *Earthquake source Mechanics*, Maurice Ewing Volume 6, Geophysical Monograph 37, American Geophys. Union, Washington, D.C, 311-318

- Baria, R., Michelet, S., Baumgaertner, J., Dyer, B., Gerard, A., Nicholls, J., Hettkamp, T., Teza, D., Soma, N., Asanuma, H., Garnish, J., Megel, T., 2004, Microseismic monitoring of the world's largest potential HDR reservoir, Proceedings of the 29<sup>th</sup> Workshop on Geothermal Reservoir Engineering, Stanford University, California
- Block, L., Cheng, C., Fehler, M. and Phillips, W.S., 1994, Seismic imaging using microearthquakes induced by hydraulic fracturing, *Geophysics*, Vol.59, No.1, p.102-112
- Brune, J.N., 1970, Tectonic stress and the spectra of seismic shear waves from earthquakes, *J.Geophys. Res.* 75, 4997-5009
- Fehler, M. and Phillips, W.S., 1991, Simultaneous Inversion for Q and source parameters of microearthquakes accompanying hydraulic fracturing in granitic rock, *Bull. Seism. Soc. Am.* 81, 553-575
- Gaucher, E., Cornet, F., and Bernard, P., 1998, Induced seismicity analysis for structure identification and stress field determination, Paper SPE 47324, Proc. SPE/ISRM, Trondheim, Norway
- Got, J.-L., Frechet, J., Klein, F., 1994, Deep fault plane geometry inferred from multiplet relative relocation beneath the south flank of Kilauea, *Journal of Geophysical Research*, v. 99, p. 15,375-15,386.
- Healy, J.H., Rubey, W.W., Griggs, D.T. and Raleigh, C.B., 1968, The Denver Earthquakes, *Science*, Volume 161, Number 3848, 1301-1310
- Hettkamp, T., Klee, G. and Rummel, F., 1998, Stress regime and permeability at Soultz derived from laboratory and in situ tests, 4<sup>th</sup> Int. HDR Forum Strasbourg
- Jones, R. H. and Evans, K. F., 2001, Improved source parameter estimates for microseismic events occurring during the 1993 injections of GPK1 at Soultz-sous-Forêts, *Technical report to New Energy Development Organization (NEDO) for Swiss contribution to the Murphy project for FY2000*
- Li, Y., Cheng, C. and Toksöz, N., 1998, Seismic monitoring of the growth of a hydraulic fracture zone at Fenton Hill, New Mexico, *Geophysics*, V. 63, No.1, p.120-131
- Madariaga, R., 1976, Dynamics of an expanding circular fault, *Bull. Seism. Soc. Am.*, v. 66, 639-666
- McGarr, A., 1976, Seismic moments and volume changes, *Journal of geophysical research*, 81, n°8, 1487-1494
- Michelet, S., Baria, R., Baumgaertner, J., Gerard, A., Oates, S., Hettkamp, T. and Teza, D., 2003, Seismic source parameter evaluation and its importance in the development of an HDR/EGS system, Proceedings of the 29<sup>th</sup> Workshop on Geothermal Reservoir Engineering, Stanford University, California
- Moriya, H., Nagano, K. and Nitsuma, H., 1994, Precise source location of AE doublets by spectral matrix analysis of triaxial hodogram, *Geophysics*, v. 59, p. 36-45.
- Moriya, H., Nakazato, K., Nitsuma, H. and Baria, R., 2002, Detailed fracture system of the Soultz-sous-Forêts HDR field evaluated using microseismic multiplet analysis, *Pure appl. Geophys.*, v. 159, p. 517-541.
- Nicholson, C. and Wesson, R.L., 1992, Triggered Earthquake and Deep Well Activities, Special Issue on Induced Seismicity, A. McGarr, ed., *PAGEOPH*, 139, n°3-4

Phillips, W.S., House, L. and Fehler, M., 1997, Detailed joint structure in a geothermal reservoir from studies of induced microearthquake clusters, JGR, v. 102, No. B6, p11745-11763

Poupinet, G., Ellsworth, W., Frechet, J., 1984, Monitoring velocity variations in the crust using earthquake doublets: an application to the Calaveras fault, California, Journal of Geophysical Research, v. 89, No. B7, p. 5719-5731

Tezuka, K., and Nitsuma, H., 1997, Integrated interpretation of microseismic clusters and fracture system in a hot dry rock artificial reservoir, SEG Expanded Abstracts, 657-660



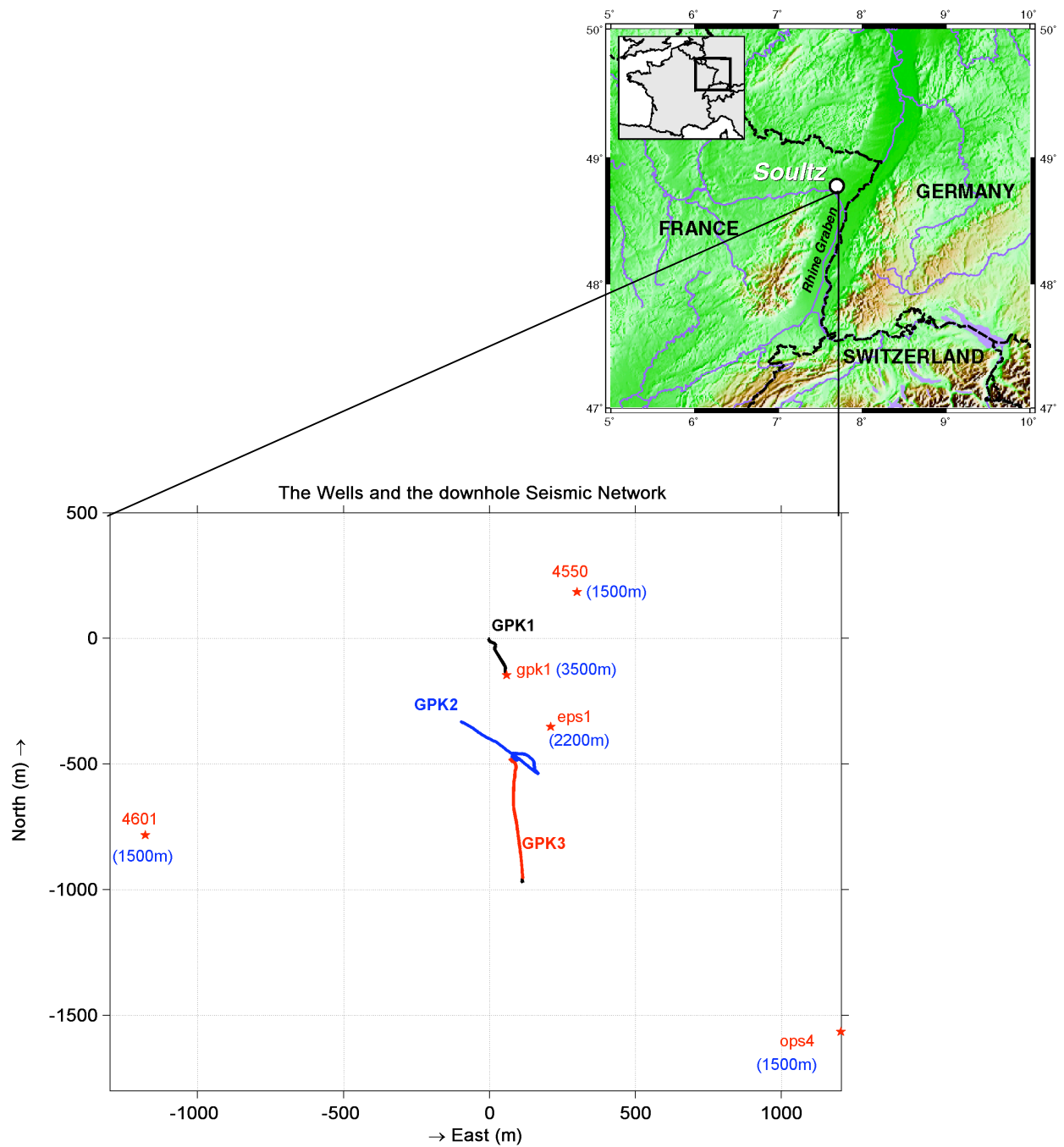


Figure 1: The top figure shows the location of the site. The bottom figure represents a plan view of the three injection wells: GPK-1, GPK-2 and GPK-3 and the downhole seismic network (stars represent the positions of the seismic stations and numbers in brackets are their depths).

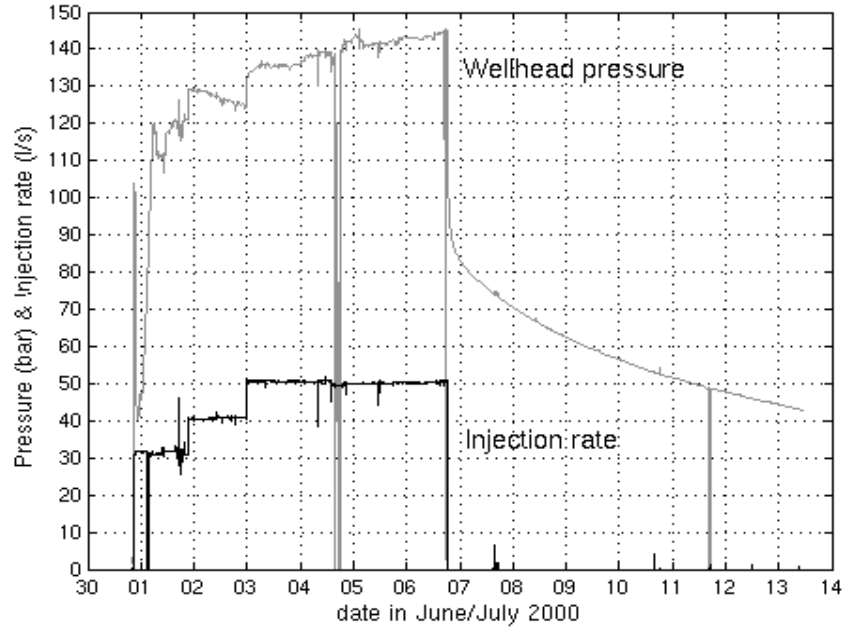


Figure 2a: Wellhead pressure in bars and Injection rate in l/s as a function of time during the stimulation done in 2000 in Soultz-sous-Forêts.

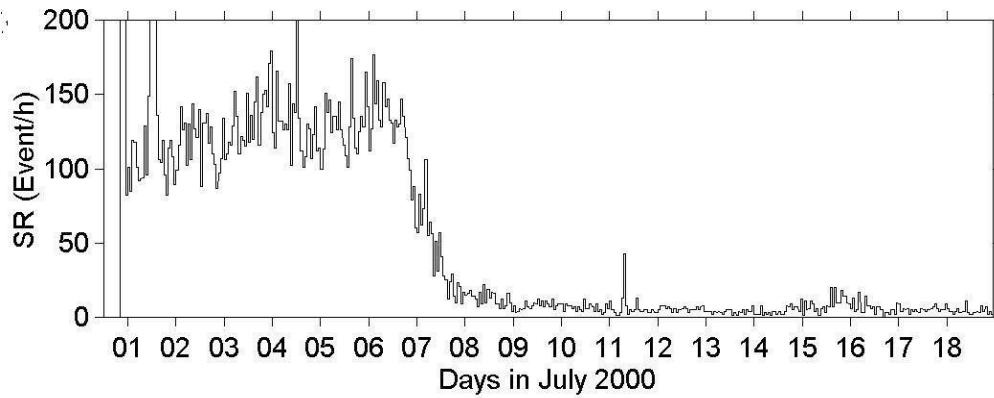


Figure 2b: Seismic rate (number of events per hour) as a function of time during and after the stimulation.

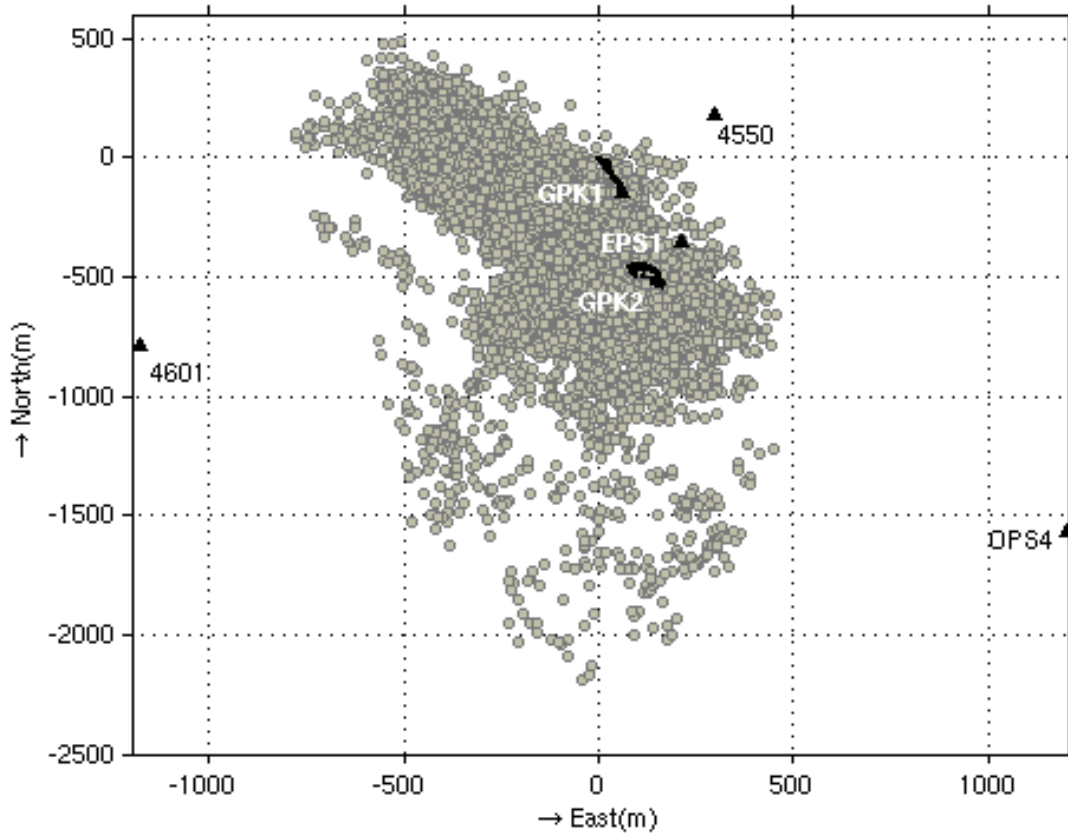


Figure 3: Plan view of the seismic monitoring wells and the microseismic cloud from the 2000 stimulation. Seismic sensors were deployed at depth in wells GPK1, 4550, EPS1, OPS4 and 4601. Note that the seismic cloud trends Northwest of the well GPK2 and extends from the casing shoe (i.e. 4430m) to 5500m depths.

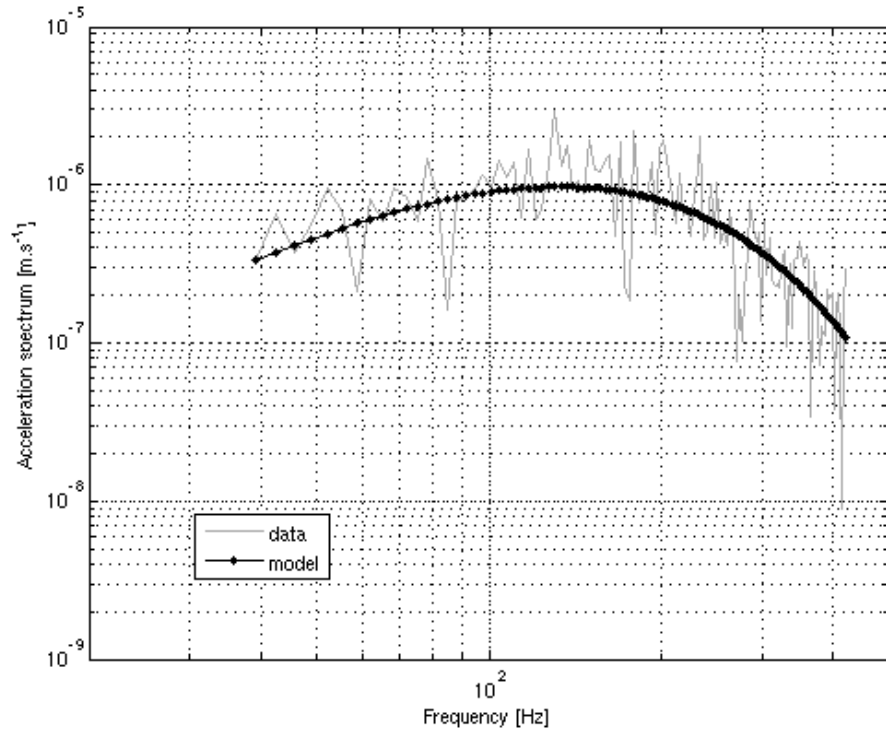


Figure 4: Acceleration spectrum ( $\text{m.s}^{-1}$ ) as a function of the frequency (Hz). The observed data are fitted with equation (2), which is represented by a dotted black curve.

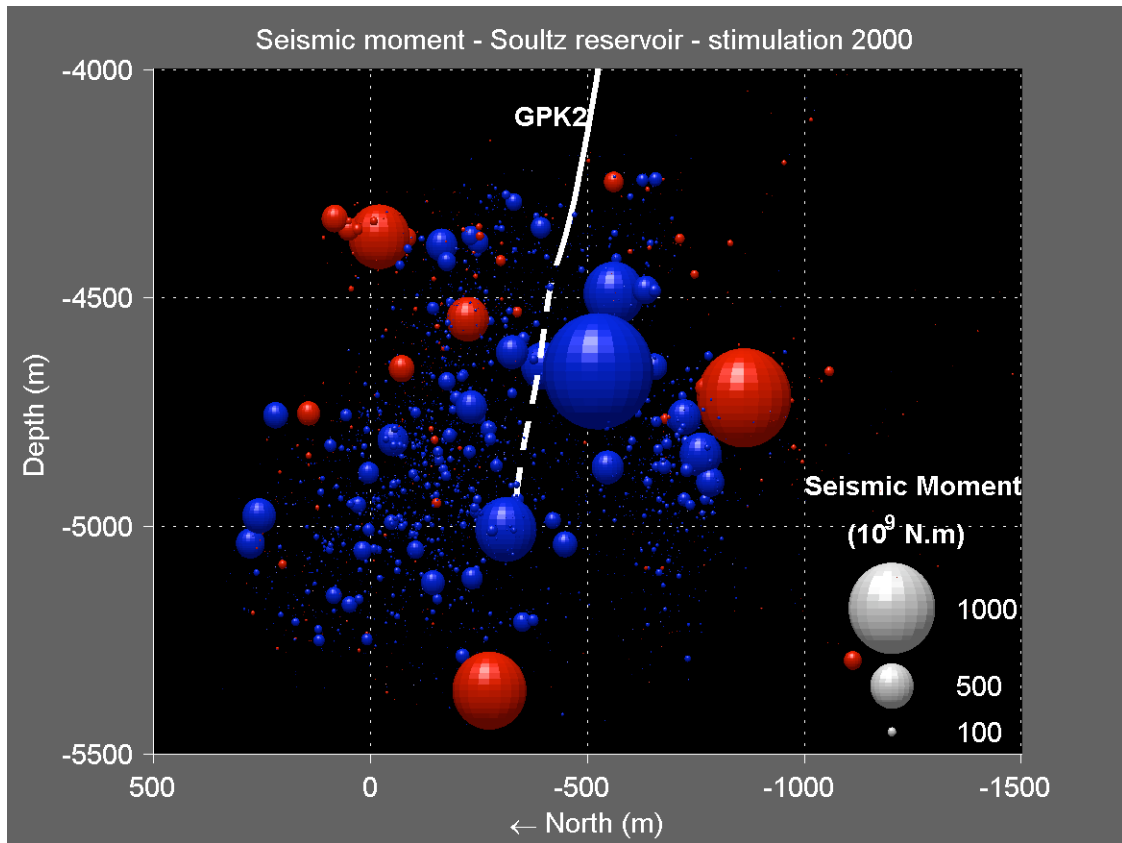


Figure 5: Vertical view of the seismic moments for microearthquakes occurring during the 2000 stimulation (blue) and after the shut-in (red). The radii of the spheres are proportional to the seismic moments.

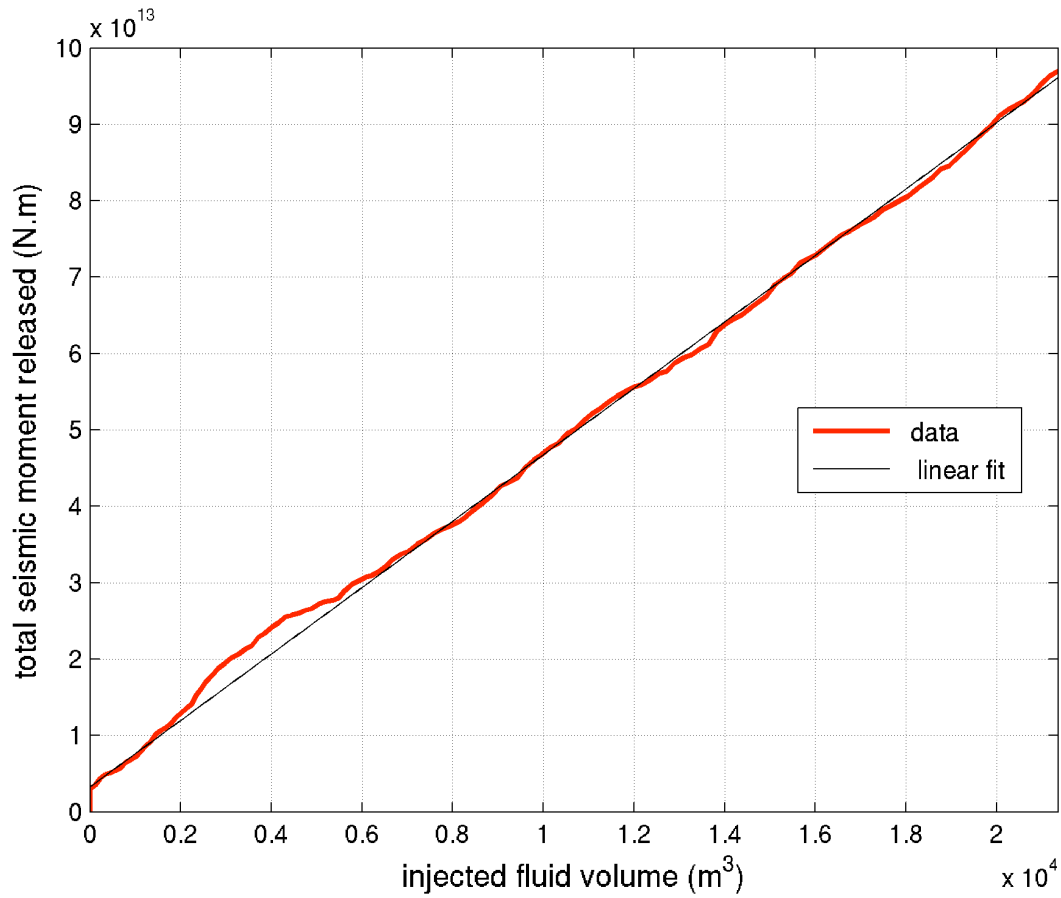


Figure 6: Total seismic moment (N.m) as a function of the injected fluid volume (m<sup>3</sup>). A linear relation, represented by a black thin line, is found to fit the observation (red line).

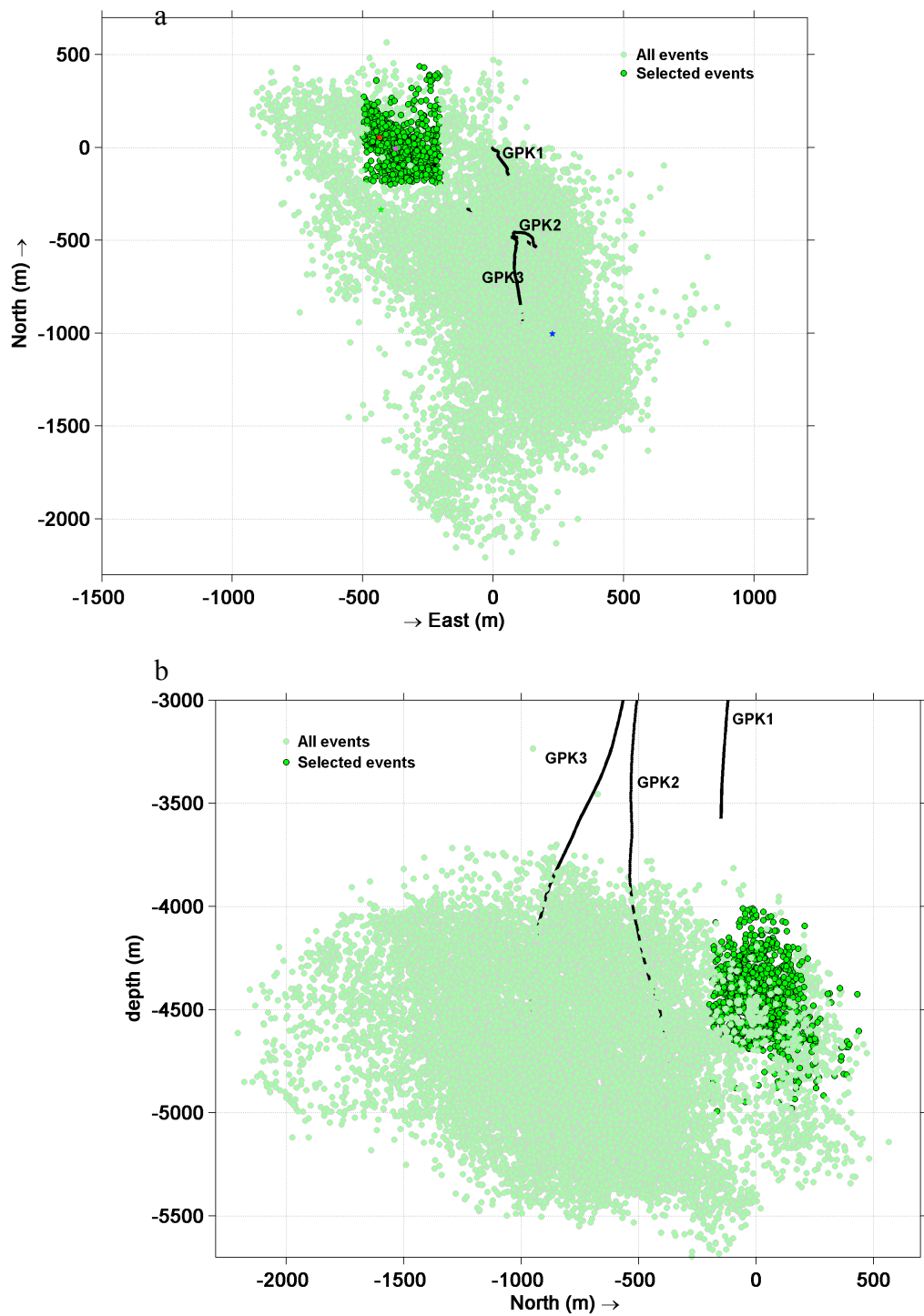


Figure 7: Top view (a) and Vertical view (b) of the seismicity associated with the stimulation in 2003 – The dots represents all the microseismic events and the dark green dots represents the events selected for the multiplet analysis.

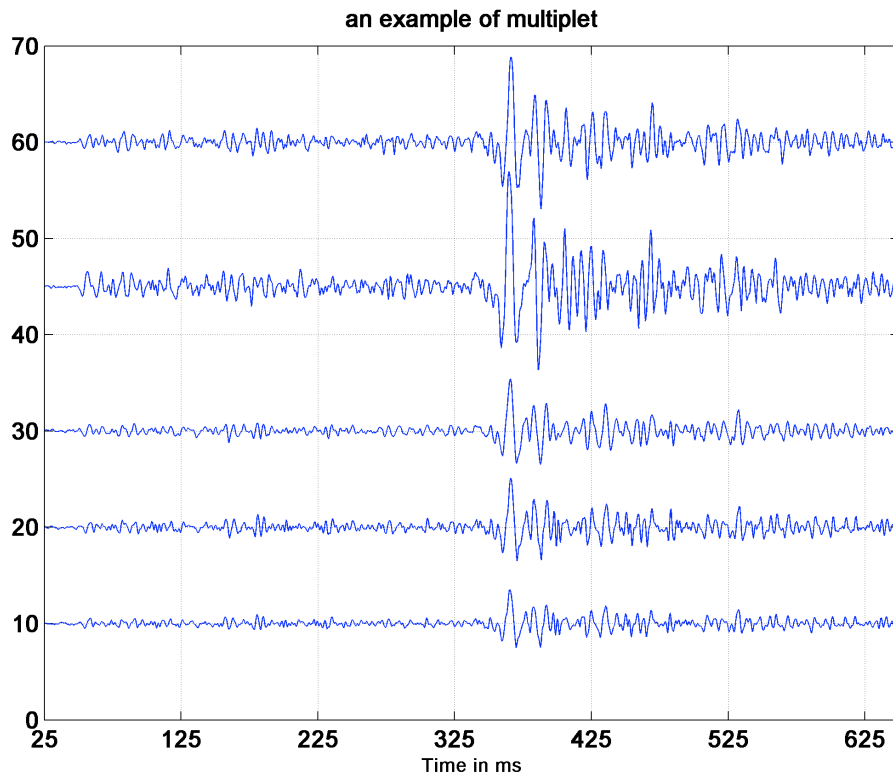


Figure 8: Seismic waveforms - example of a multiplet composed of 5 microearthquakes



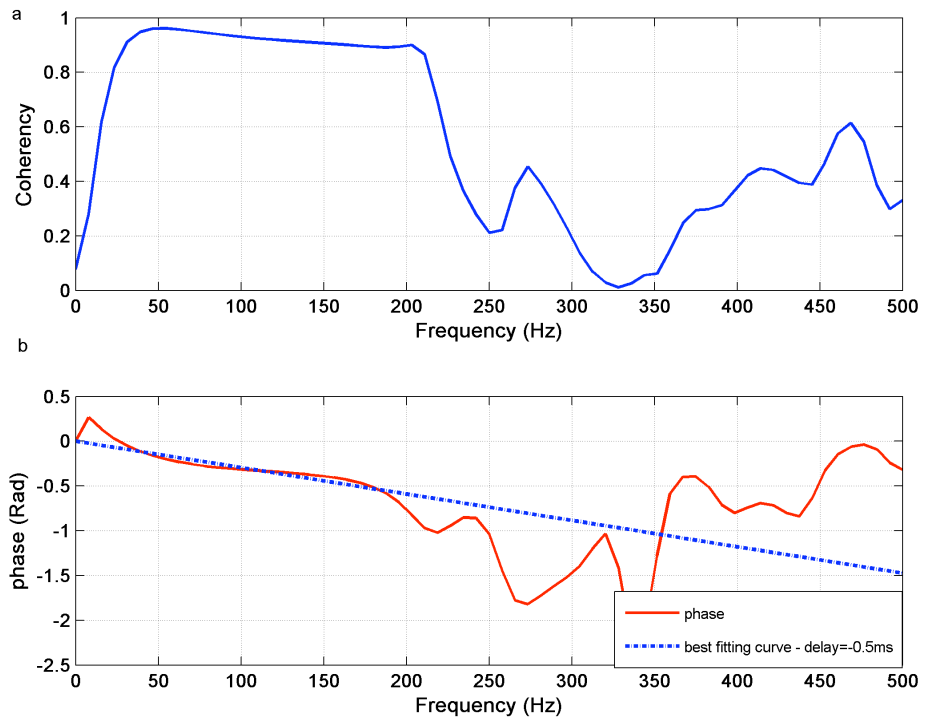


Figure 9: a) Coherency as a function of the frequency b) Phase as a function of the frequency

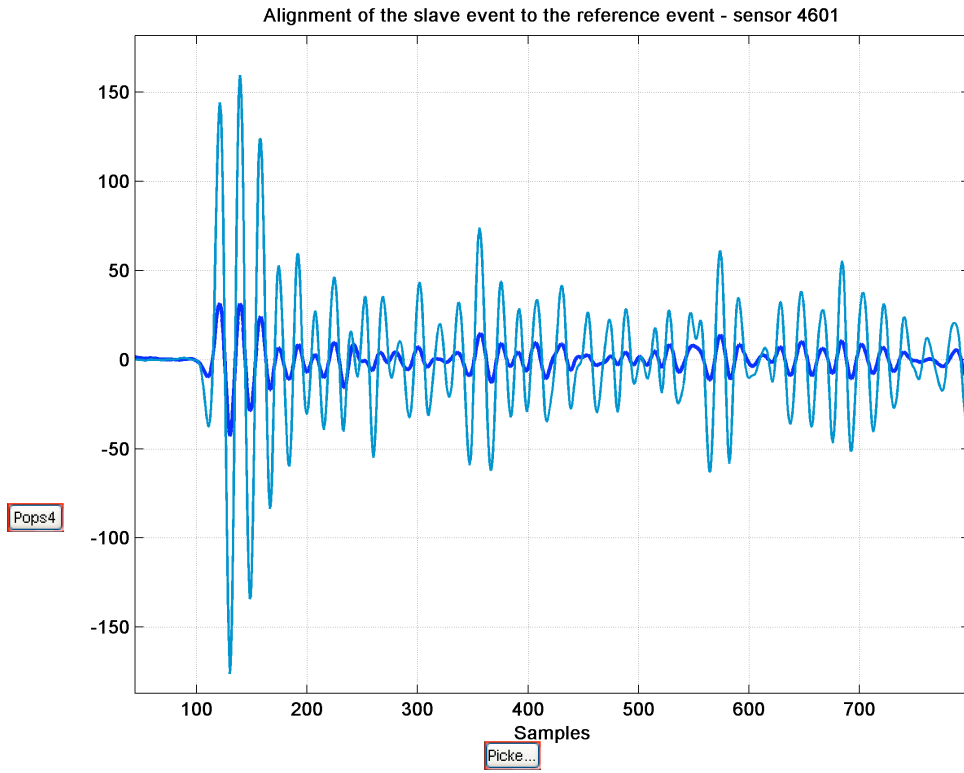


Figure 10: Alignment of the reference seismic trace and its slave

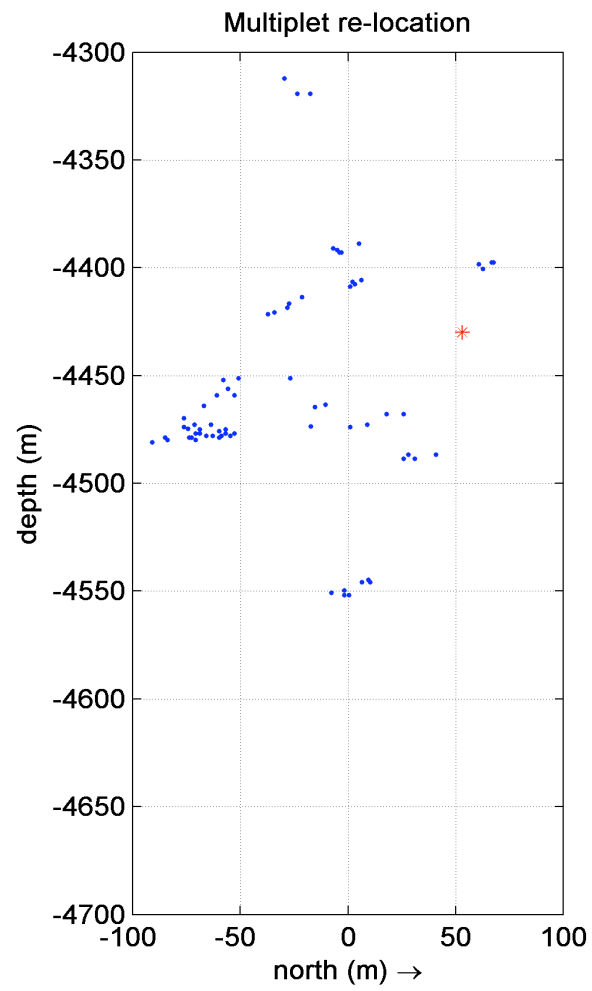


Figure 11: Vertical view of the relocated clusters - the asterisk represents an earthquake with magnitude larger than 2.5

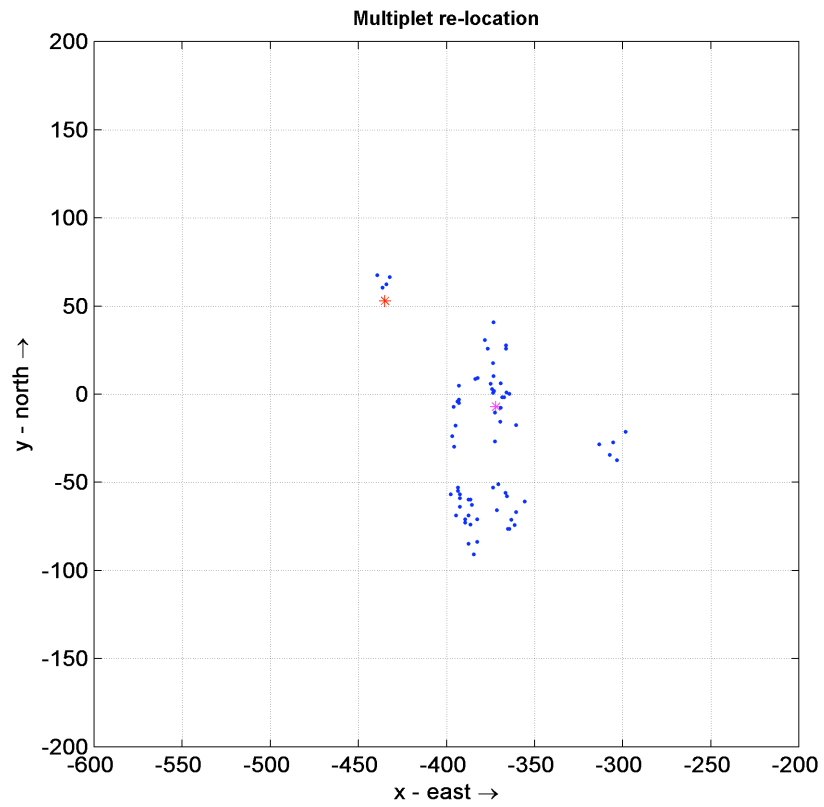


Figure 12: Map view of the relocated clusters – the asterisks represent earthquakes with magnitude larger than 2.5

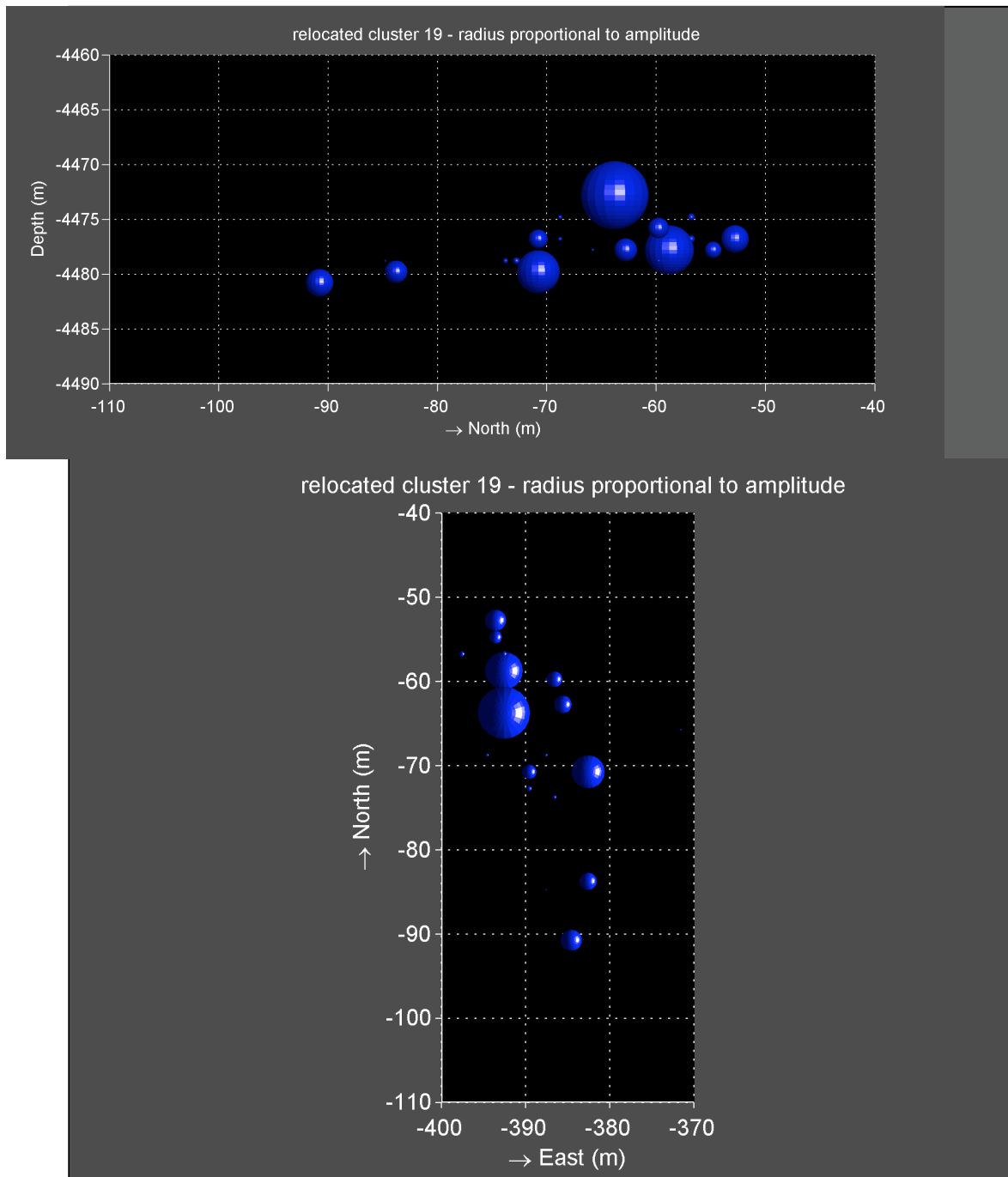


Figure 13: Vertical view (top) and map view (bottom) of the cluster composed of 19 events - spheres have radius proportional to the amplitude of the earthquake